ISSN 0031-918X, The Physics of Metals and Metallography, 2013, Vol. 114, No. 6, pp. 488–502. © Pleiades Publishing, Ltd., 2013.
Original Russian Text © V.G. Pushin, N.N. Kuranova, N.I. Kourov, R.Z. Valiev, A.V. Korolev, V.V. Makarov, A.V. Pushin, A.N. Uksusnikov, 2013, published in Fizika Metallov i Metallovedenie, 2013, Vol. 114, No. 6, pp. 534–548.

STRUCTURE, PHASE TRANSFORMATIONS, AND DIFFUSION

Effect of Heat Treatment on Structural and Phase Transformations in the $Ti_{49.5}Ni_{50.5}$ Alloy Amorphized by High-Pressure Torsion

V. G. Pushin[a, b], N. N. Kuranova[a], N. I. Kourov[a], R. Z. Valiev[c], A. V. Korolev[a], V. V. Makarov[a], A. V. Pushin[a, b], and A. N. Uksusnikov[a]

[a] *Institute of Metal Physics, Ural Branch, Russian Academy of Sciences, ul. S. Kovalevskoi 18, Ekaterinburg, 620990 Russia*
[b] *The First President of Russia B. N. Yeltsin Ural Federal University, ul. Mira 19, Ekaterinburg, 620002 Russia*
[c] *Institute of Physics of Advanced Materials, ul. K. Marksa 12, Ufa, 450000 Russia*
e-mail: pushin@imp.uran.ru

Received August 8, 2012; in final form, December 11, 2012

Abstract—Results are presented for a study of the structural and phase transformations that occur in the titanium-nickelide shape-memory alloy $Ti_{49.5}Ni_{50.5}$ subjected to heat treatment after deformation-induced amorphization by megaplastic high-pressure torsion (HPT) using five or ten revolutions of Bridgman anvils. The investigations were performed using transmission and scanning electron microscopy, X-ray diffraction, and measurements of the temperature dependences of electrical resistivity and magnetic susceptibility. It has been established that the crystallization of the alloy already occurs upon low-temperature treatment, beginning with ~500 K. The evolution of the structure and the stage character of the development of crystallization and recrystallization processes depending on temperature have been determined. It has been shown that the annealing of the amorphized alloy makes it possible to obtain highly homogeneous nanostructured, submicrocrystalline, or bimodal states in the *B*2 austenite. A complete diagram of thermoelastic martensitic transformations of the *B*2 austenite has been constructed in the region from a nanostructured to a conventional polycrystalline state (with a grain size of 20–50 μm). The effect of size on the stabilization of austenite has been revealed and its specific features have been studied for the $B2 \rightarrow R$ and $B2(R) \rightarrow B19'$ martensitic transformations depending on the structural state of the alloy.

Keywords: martensitic transformations, structural and phase transformations, titanium nickelide (TiNi), shape-memory effect

DOI: 10.1134/S0031918X13060124

INTRODUCTION

Atomically ordered titanium-nickelide-based alloys, which undergo thermoelastic martensitic transformations (TMTs) upon changes in temperature and pressure or in the process of deformation, exhibit many unique and practically attractive functional and mechanical properties [1–10]. These are, first of all, one-way and all-round shape-memory effects (SMEs), transformation-induced plasticity or pseudoelasticity, deformation-induced superplasticity, and anomalously high damping ability. It has been revealed in our previous works [9–15] that, using the methods of ultrarapid quenching and megaplastic deformation, these alloys can be obtained in a high-strength nanostructured state. It has been established that various structural and phase states can be obtained in the TiNi -based alloys depending on the technology of their preparation, such as single-crystal or polycrystalline (usual microcrystalline (MC), submicrocrystalline (SMC), or nanocrystalline (NC)) single-phase or multiphase states. One of new directions in modern materials science is that in which the production of bulk nanostructured structural and functional materials, including shape-memory alloys, is provided by methods of severe plastic deformation (SPD) [16–22]. The highest degrees of deformation in experimental samples that remain intact after deformation can be obtained by the method of high-pressure torsion (HPT). The variation of the regimes of HPT and of subsequent heat treatments makes it possible to obtain TiNi-based alloys with different sizes of nanograins and different levels of physical characteristics [21–26]. This paper is devoted to investigating the effect of heat treatment on the main features of the phase and structural transformations and properties of TiNi-based alloys amorphized by HPT.

EXPERIMENTAL

As the object of the investigation, we have chosen a TiNi-based alloy of composition $Ti_{49.5}Ni_{50.5}$. The alloy was prepared from high-purity components (iodide titanium of 99.8% purity, and nickel of 99.99% purity) by electric-arc melting in the atmosphere of purified helium and was subjected to fivefold remelting and subsequent long-term homogenizing annealing in

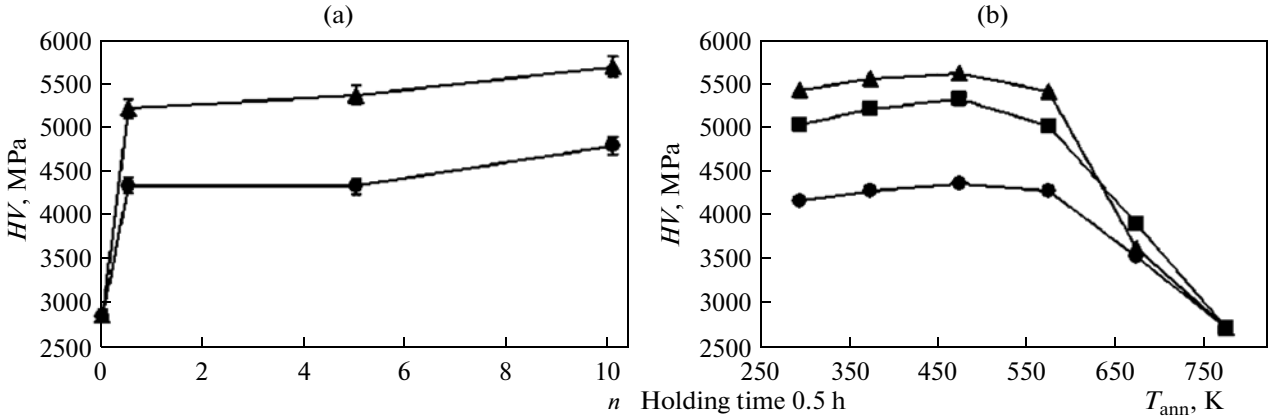

Fig. 1. Microhardness of $Ti_{49.5}Ni_{50.5}$ alloy in (a) deformed and (b) annealed states: (●) at the center of the sample; (▲) at the edge of the sample; and (■) at the mid-radius.

argon at a temperature of 1073 K. The average grain size in the alloy could be varied in the optimum range of 30 to 50 μm. The temperatures of the start (M_s, A_s) and finish (M_f, A_f) of the forward (M_s, M_f) and reverse (A_s, A_f) $B2 \leftrightarrow B19'$ martensitic transformation, as determined from the temperature dependences of electrical resistivity, in the alloy with a grain size of 30–50 μm quenched from 1073 K were as follows: $M_s = 278 \pm 2$ K, $M_f = 248 \pm 2$ K, $A_s = 288 \pm 2$ K, and $A_f = 308 \pm 2$ K. Consequently, at room temperature, the alloy is in the state of metastable $B2$ austenite. The samples for HPT studies were cut from cylindrical ingots in the form of disks 10 mm in diameter and 0.3 mm thick. The rotation of one of the anvils in the Bridgman chamber by five and ten turns produced a megaplastic shear deformation (e = 6.4 and 7.1, respectively) due to friction forces in the samples pressed by the anvils from both sides to a pressure of 6 GPa at room temperature. The isothermal heat treatment was performed in electrical-resistance furnaces at temperatures in the range of 373–873 K.

The structure and the phase transformations were studied by the methods of phase and structural X-ray diffraction analysis (in the copper monochromatized radiation, λ = 1.54178 Å) and by transmission and scanning electron microscopy (TEM and SEM, respectively). The electron-microscopic investigations were performed using Tecnai G^2 30, JEM 200 CX, and Quanta 200 Pegasus electron microscopes at the Department of Electron Microscopy, Institute of Metal Physics, Ural Branch, Russian Academy of Sciences (Center of Collaborative Access, Ural Branch, Russian Academy of Sciences). These methods permitted us to reliably identify the phase and chemical composition and the atomic, nanostructured, and microcrystalline structure of the initial austenitic and martensitic phases, as well as to determine the lattice parameters and their evolution in the process of deformation and temperature variation, and to obtain information on the nano- and micromorphology and fine internal structure of grains (crystallites) and martensitic crystals. The average size of grains was determined from electron micrographs by averaging data on more than 300 grains. In addition, we performed measurements of the electrical resistivity, magnetic susceptibility, hardness, and mechanical properties in wide temperature ranges.

RESULTS

As was established previously [26], after HPT by five and ten revolutions of the anvil, the $Ti_{49.5}Ni_{50.5}$ alloy is in a deformation-induced amorphized state. The amorphous matrix of the alloy is characterized by a high density of uniformly distributed nanocrystalline inclusions (3–5 nm in size) with a distorted partly ordered ($B2$-type) austenitic structure. It is also known [22–24] that the microstructural state of the alloy even after multiple treatments with HPT is by no means completely uniform along the disk radius, although it is fairly uniform over the thickness of the disk. Therefore, we first performed characterization-type X-ray diffraction investigations and measurements of the electrical resistivity, magnetic susceptibility, and microhardness (measured along the disk radii) using samples cut from various (middle and peripheral) regions of the disks (Fig. 1). It can be seen that, depending on the number of the anvil revolutions during the HPT and on the position of the microhardness indentation on the disk, the values of the microhardness vary in a significant range of 4.5–5.5 GPa. Based on these data, all subsequent experiments were performed on two series of samples cut from the central and peripheral regions of disks subjected to HPT.

It is natural that amorphous alloys are stable when being cooled in the cryogenic temperature range. However, since even after HPT with five and ten revolutions of the anvil, the alloy is not completely homogeneous and contains numerous nanocrystals, we performed additional low-temperature investigations

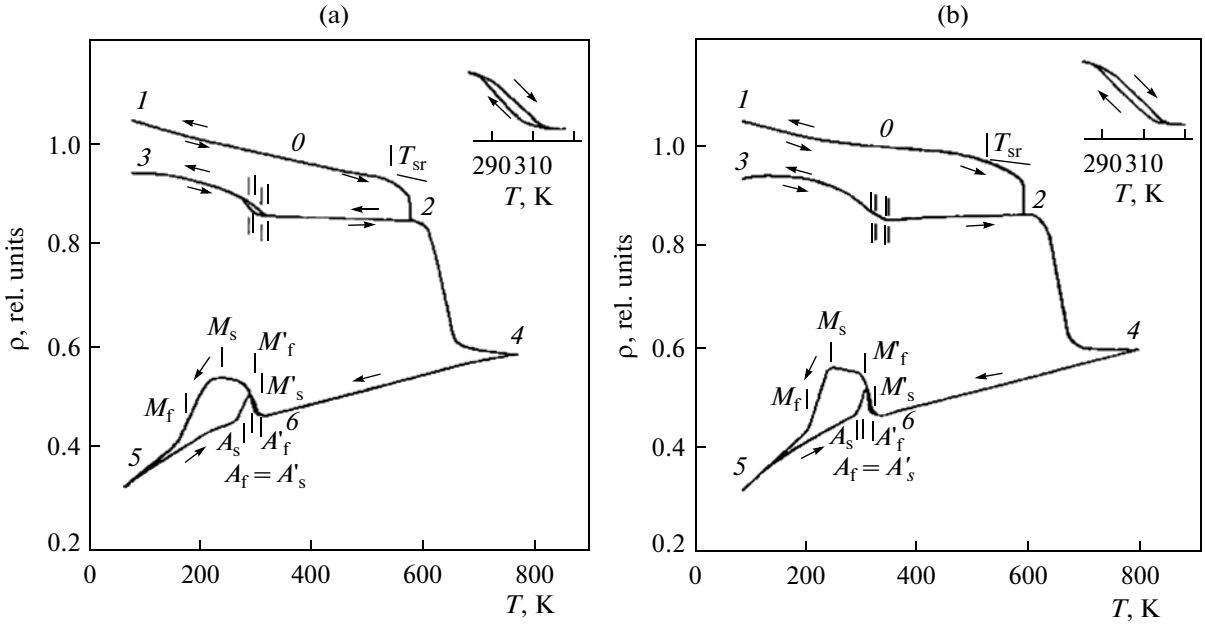

Fig. 2. Temperature dependences of electrical resistivity of $Ti_{49.5}Ni_{50.5}$ alloy subjected to HPT ($n = 5$ rev, $P = 6$ GPa): (a) at the edge of the sample; (b) at the center of the disk; (*0*)the temperature of the onset of measurements (room temperature); (*1*, *3*, *5*) boiling temperature of liquid nitrogen, T_N; (*2*) temperature of 573 K; (*4*) 773 K; and (*6*) final temperature of measurements, 323 K.

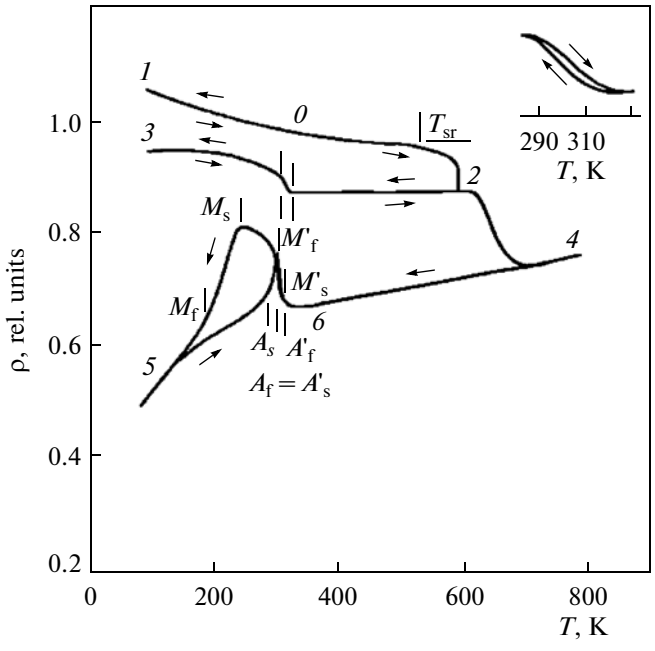

Fig. 3. Temperature dependence of electrical resistivity of $Ti_{49.5}Ni_{50.5}$ alloy subjected to HPT ($n = 10$ rev, $P = 6$ GPa) at center of the disk: (*0*) temperature of the boiling temperature of measurements (room temperature); (*1*, *3*, *5*) boiling temperature of liquid nitrogen, T_N; (*2*) temperature equal to 573 K; (*4*) 773 K; and (*6*) final temperature of measurements, 323 K.

using methods that are highly sensitive to structural and phase transitions in the alloy. To establish the possibility of the occurrence of martensitic transformations and to quantitatively determine their critical temperatures, measurements of the temperature dependences of the electrical resistivity $\rho(T)$ and magnetic susceptibility $\chi(T)$ are especially sensitive and fairly rapid methods. Figures 2 and 3 show kinetic curves of the variation of $\rho(T)$ for the alloy samples cut from the middle and periphery regions and subjected to HPT with five and ten revolutions of the anvil, respectively. The $\rho(T)$ measurements were performed sequentially for all the samples according to the following route: cooling from room temperature (*RT*) to the boiling temperature of liquid nitrogen (T_N); then, heating to 573 K (with a holding for 20 min) and cooling to T_N; heating to 773 K; cooling to T_N; and warming to 323 K. The monotonic variation of $\rho(T)$ in the first portion of the route (0–1) means that no phase and structural transformations occur upon cooling to T_N. The subsequent heating of the amorphized alloy to relatively low temperatures (480–500 K) leads to the onset of crystallization, which is noted by the points T_{sr} in Figs. 2 and 3.

It was revealed by electron-microscopy that, upon annealing in a wide temperature range, one can easily achieve nanocrystalline states that consist of equiaxed nanograins highly homogeneous in size in amorphous TiNi-based alloys. According to TEM data, after annealing at 473 K for 20 min there begins nanocrystallization of the alloy with the formation of nan-

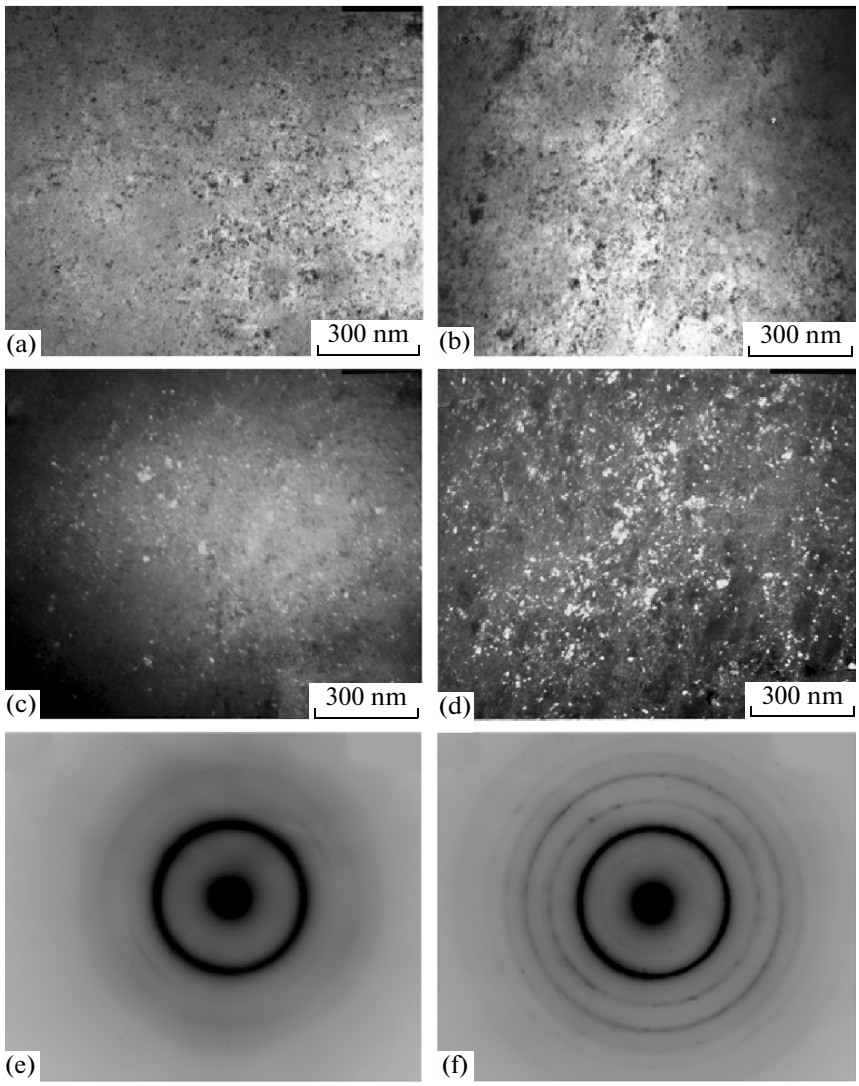

Fig. 4. (a, b) Bright-field and (c, d) dark-field micrographs and (e, f) electron diffraction patterns of the $Ti_{49.5}Ni_{50.5}$ alloy subjected to HPT (b, d, f) $n = 5$ rev or (a, c, e) $n = 10$ rev at 6 GPa + annealing at 473 K for 20 min: (a, c, e) at the edge of the disk and (b, d, f) at the center of the disk.

ograins with dimensions of 10–20 nm (Figs. 4a, 4b). In the corresponding selected-area diffraction (SAED) patterns, continuous distributions of numerous merging fundamental and superstructure reflections of the *B*2 phase can be seen against the background of a strong diffuse halo from the amorphous matrix near the 110_{B2} ring, as well as other reflections (Figs. 4e, 4f). Therefore, when taken in strong diffraction rings, numerous isolated nanocrystallites are shining in dark-field micrographs; the average size and density of these nanocrystallites are somewhat greater in the sample cut from the middle part of the disk (cf. Figs. 4c and 4d).

After annealing at 523 K for 20 min, an increase in the size (within 15–25 nm) is observed, especially in the density of the nanograin distribution, which is demonstrated by typical bright-field and dark-field micrographs and SAED patterns shown in Figs. 5a–5c. In the SAED patterns, the ringlike intensity distributions become much sharper and begin to exhibit some texture-like discreteness in the disposition of the reflections. An analysis shows that, in the alloy, a nanocrystalline *B*2 structure is formed, which is now substantially more homogeneous in the size of nanograins and in their distribution over the volume of the sample, which is supported by the high-resolution electron-microscopic images (direct resolution of the atomic lattice, see Figs. 5d, 5e). In Fig. 5e, regions located near the boundaries of nanocrystallites are delineated schematically by solid lines. Within these regions (2–3 interatomic spacings wide), local bends (or jumps) are clearly seen in the contrast at coherent (or partly coherent) interfaces between the nanocrystallites. In these images, the boundaries of grains and subgrains

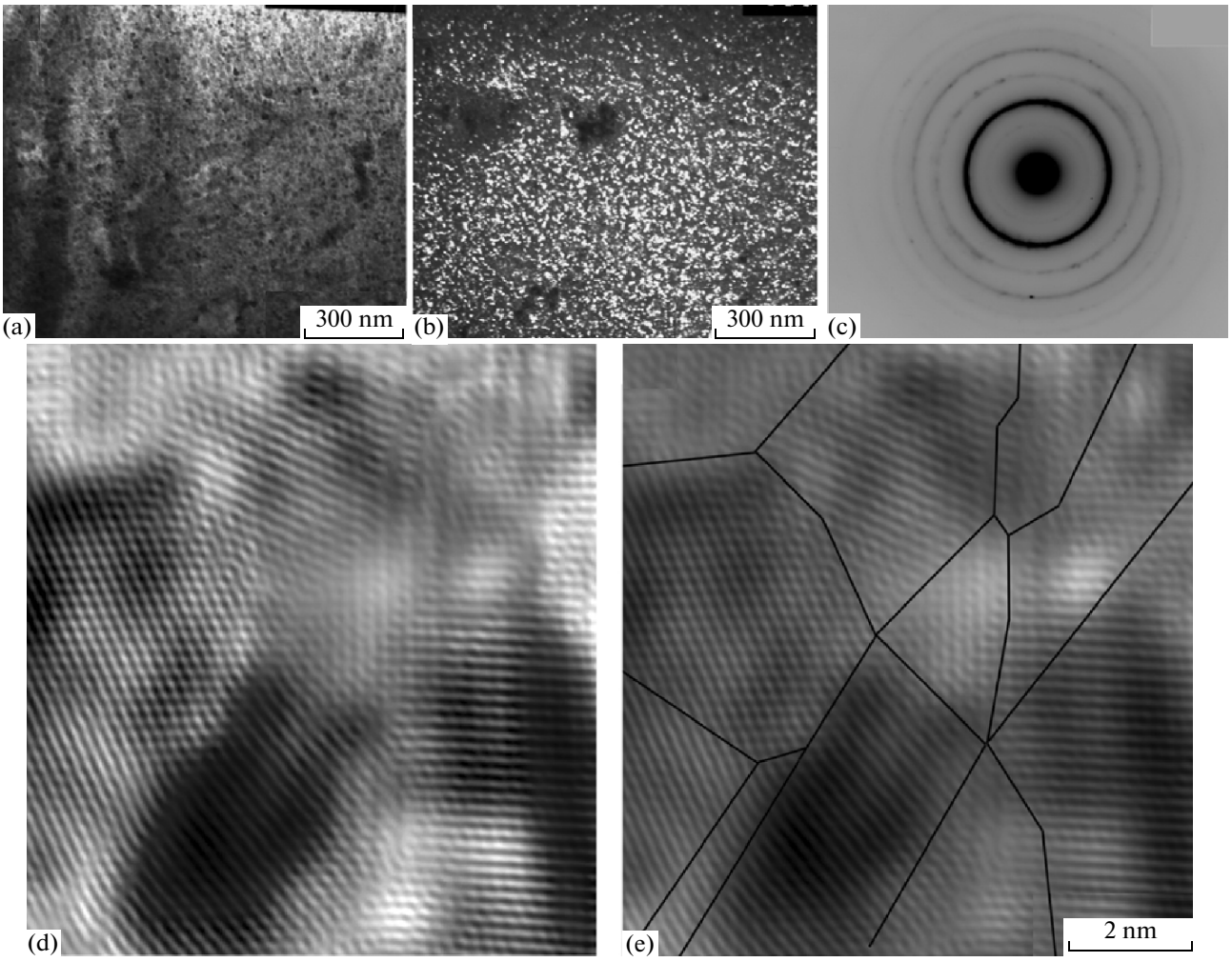

Fig. 5. (a) Bright-field and (b) dark-field micrographs (amplitude contrast), (c) corresponding electron diffraction pattern, and (d, e) micrographs of the direct atomic resolution (phase contrast) of the $Ti_{49.5}Ni_{50.5}$ alloy subjected to HPT (n = 5 rev, P = 6 GPa + annealing at 523 K for 20 min; center of the disk).

with high- and low-angle misorientations are usually determined based on the data on the recognition of the boundaries at which changes occur in the directions of parallel rows of phase atomic contrast from neighboring crystallites.

The nanocrystalline structure that is formed as a result of annealing at 573 K (Figs. 6a, 6c, 6e) for 20 min is characterized at room temperature by somewhat greater values of the average size of equiaxed grains (30 and 50 nm, respectively). The ringlike character of the distribution of Bragg reflections is also retained after annealing at 723 and 773 K for 20 min, which leads to the formation of austenite grains with dimensions of 60–70 nm (see Figs. 6e, 6f). However, after 20-min annealing at 823 and 873 K or with increasing holding duration at 723 and 773 K to 1 h, the alloy exhibits numerous regions with noticeably greater sizes of grains (more than 150–200 nm) while retaining a significant fraction of highly dispersed nanograins (less than 100 nm); therefore, in the case of this bimodal morphology, the average grain size increases sharply, being equal to 100 and 180 nm after annealing for 20 min at 823 and 873 K, respectively (Figs. 7a, 7b). The even greater average size of $B2$ grains (to 400–450 nm) is observed in the alloy after annealing at 923 K for 20 min (Figs. 7c–7f).

The single-modal or bimodal character of the $B2$-austenite microstructure formed upon annealing affects the morphology of martensite arising upon the thermoelastic martensitic transformation (cf. Figs. 6 and 7). It has been shown in TEM experiments in situ upon cooling to below room temperature that, in the NC grains, single-crystal R martensite is formed (Fig. 6c), then $B19'$ martensite (Figs. 6d, 7b); in the SMC grains, single-packet pairwise-twinned martensite arises (Figs. 7d–7f); and, in the MC grains, multipacket martensite is observed [2, 6].

Some data on the kinetics and parameters of structural and phase transformations can be obtained not only from the $\rho(T)$ and $\chi(T)$ dependences, but also

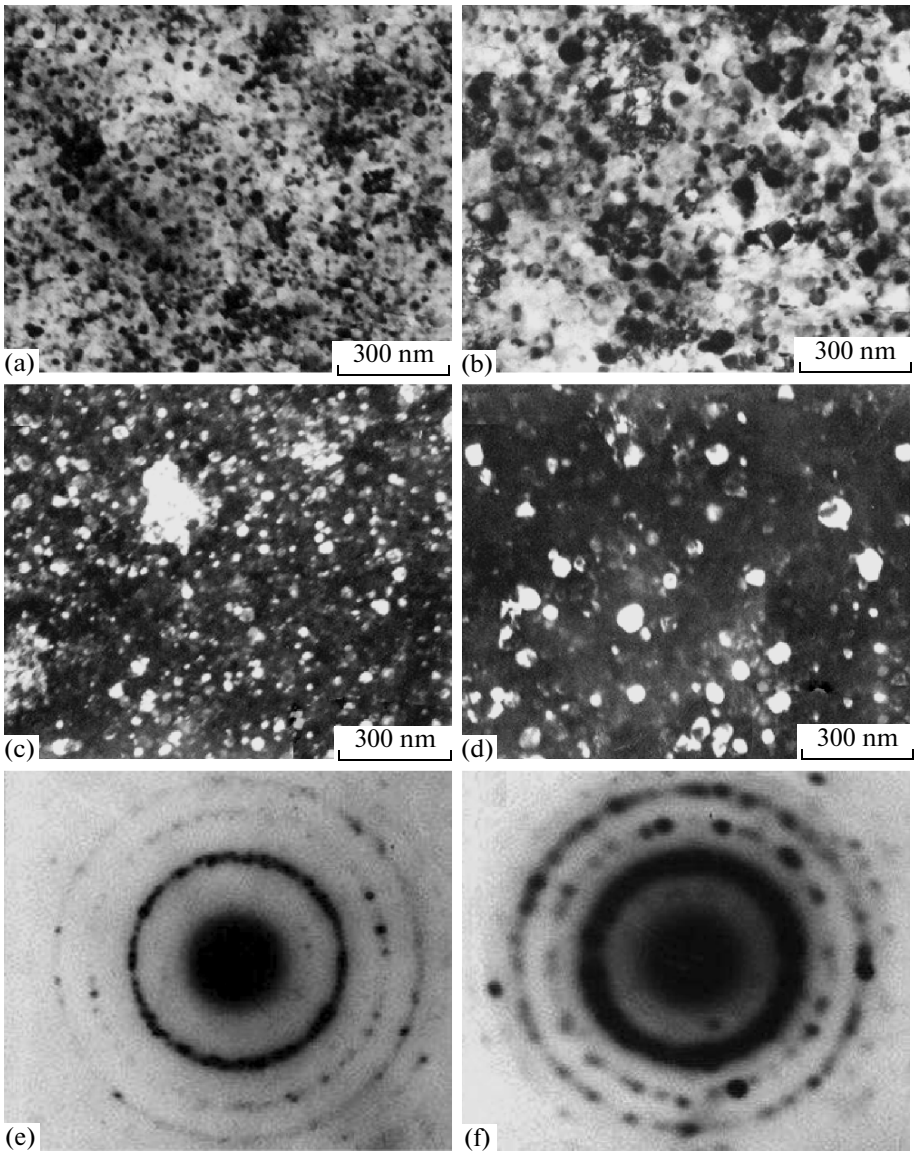

Fig. 6. (a, b) Bright-field and (c, d) dark-field micrographs and (e, f) corresponding electron diffraction patterns of the $Ti_{49.5}Ni_{50.5}$ alloy subjected to HPT ($n = 5$ rev, $P = 6$ GPa) followed by annealing (a, c, e) at 573 K for 20 min and (b, d, f) at 773 K for 5 min. Obtained upon cooling in situ to (b, e) 273 K and (d, f) 173 K.

from the investigations of the alloy subjected to HPT by differential scanning calorimetry (DSC) in the course of heating and cooling. Figure 8 displays DSC curves obtained for an almost completely amorphous $Ti_{49.5}Ni_{50.5}$ alloy subjected to HPT with five revolutions of the anvil upon heating from room temperature to 1000 K at a rate of 0.67 K/s (40 K/min). It is clearly seen from the DSC curve that the process of nanocrystallization of the amorphized matrix starts at 500 K and is in fact completed at 630 K (judging from the exothermic peak appearing at this temperature); upon further heating, the competitive growth of $B2$ grains occurs, which exhibits a clear three-stage character. Undoubtedly, the parameters of the processes of crystallization and subsequent recrystallization depend on the temperature-kinetic conditions of their realization.

DISCUSSION

As was noted above, the electron-microscopic and X-ray diffraction experiments in situ have shown that upon cooling and heating the alloy studied in the nanostructured state in fact undergoes the same type and sequences of martensitic transitions as their initial prototype in the aged state, i.e., $B2 \leftrightarrow R \leftrightarrow B19'$ (see Figs. 6, 7). Although, generally speaking, in a quenched alloy, upon cooling to below room temperature, a single transition of the $B2 \leftrightarrow B19'$ type takes

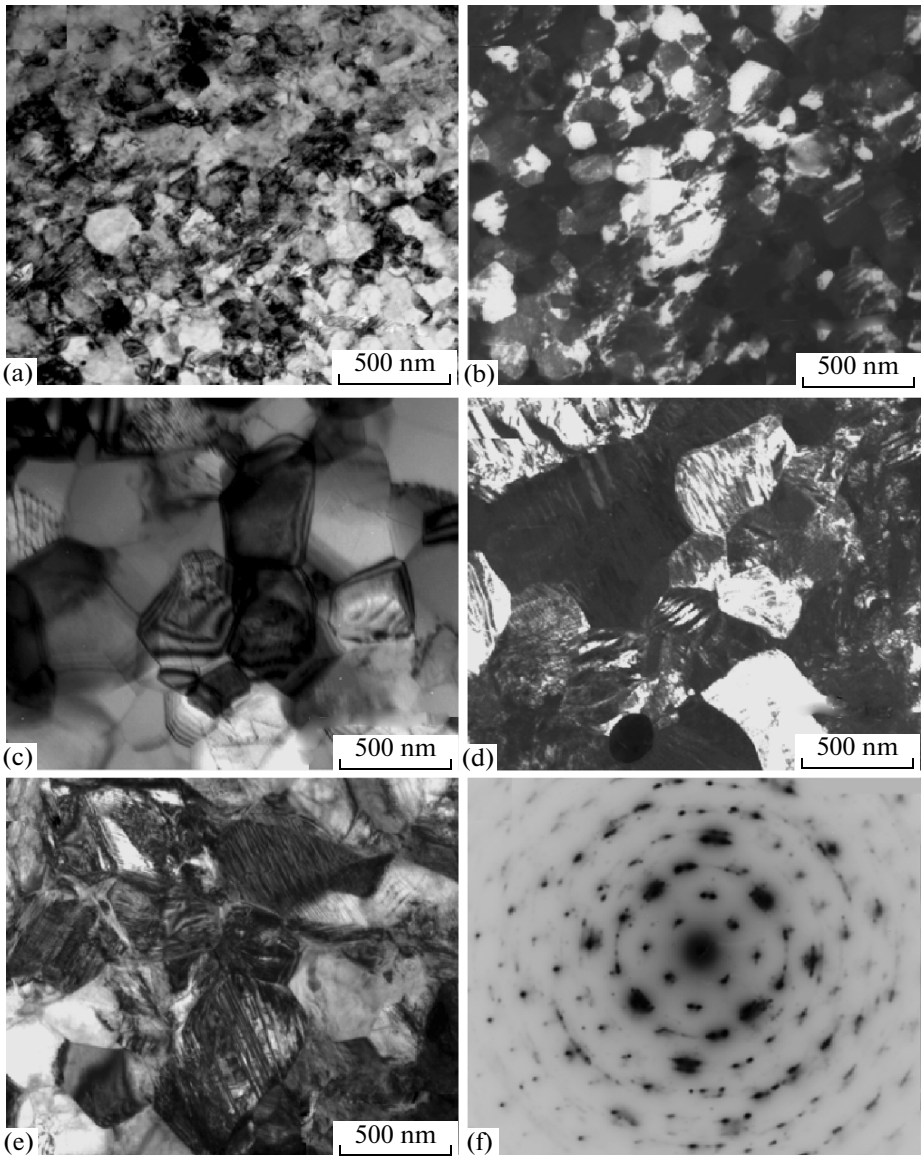

Fig. 7. (a, c, e) Bright-field and (b, d) dark-field micrographs and (f) corresponding electron diffraction pattern of the $Ti_{49.5}Ni_{50.5}$ alloy subjected to HPT ($n = 5$ rev, $P = 6$ GPa) followed by annealing (a, b) at 823 K for 20 min and (c–f) at 923 K for 20 min. Obtained (a, c) at room temperature or upon cooling in situ to (b, d–f) 173 K.

place [2, 6]. Based on the data obtained, it follows, first, that the quasi-isotropic spatial compensation of accommodation of elastic stresses induced by a shear TMT in nanostructured TiNi alloys is achieved due to not only twinning and not only in separate nanograins but also in much larger microvolumes, e.g., in large groups of neighboring grains whose ensembles form a self-accommodating elastically soft system. Second, and this is also quite important, the absence of internal twinning in the nanograins of the *R* and *B*19' martensites can serve as an experimental proof for the self-rearrangement of the austenite lattice into the martensite lattice via pure shear. But this means that the packet-type *R* twins observed in larger grains and single crystals in the $\{110\}_{B2}$ and $\{100\}_{B2}$ systems of planes of the initial austenite and the so-called geometrically necessary *B*19' microtwins of type I ($\{11\bar{1}\}_{B19'}$) and type II ($\langle 110\rangle_{B19'}$, type II) are not transformation twins [1–7]. They arise just like the composite deformation nanotwins of the $(001)_{B19'}$ type, i.e., due to the adaptive relaxation process of the secondary coherent elastic-plastic deformation by shear with an invariant lattice in the martensitic state and, naturally, in larger grains, when the absolute values of homogeneous deformations that are stored upon the transformation in a single grain become significantly greater. However, even in this case, first, a single-packet martensite is observed and

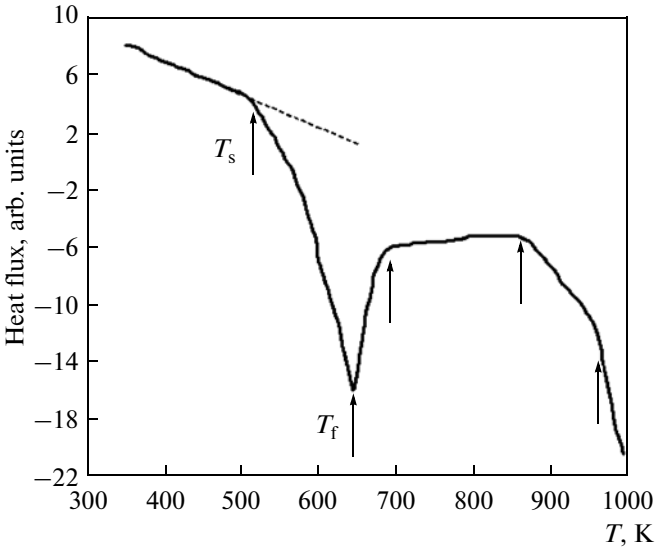

Fig. 8. Temperature dependence of heat flux during differential scanning calorimetry of the $Ti_{49.5}Ni_{50.5}$ alloy subjected to HPT ($n = 5$ rev, $P = 6$ GPa). T_s and T_f are temperatures of the start and finish of crystallization.

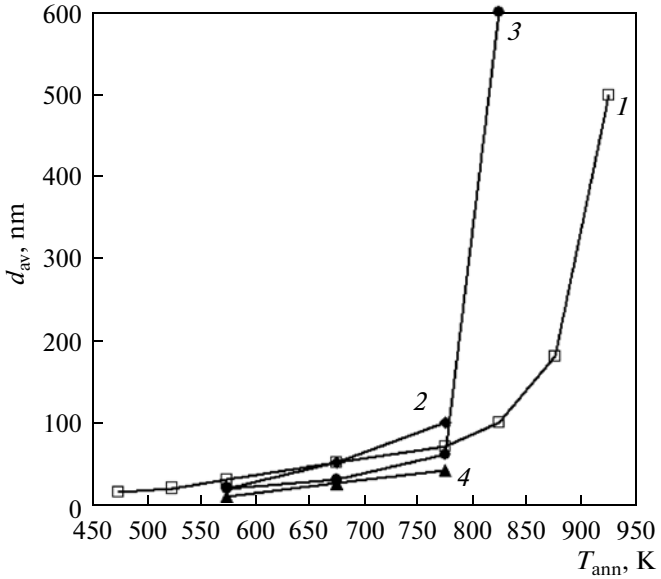

Fig. 9. Dependences of average size of grains on temperature and time of annealing of $Ti_{49.5}Ni_{50.5}$ alloy subjected to HPT with (*1*, *3*) 5 rev, (*2*) 3 rev, and (*4*) 7 rev. Annealing time: (*1*) 20 min, (*2–4*) 60 min.

only later, after the grain size becomes more than a few microns, does a multipacket martensite arise that is pairwise-twinned in the above-mentioned systems of twinning shear; this martensite is composed of crystals of corresponding crystallographically equivalent orientations defined by the requirement of the minimization of elastic stresses.

Based on an analysis of the main features of the behavior of the $\rho(T)$ dependences observed upon heating and cooling, along with the results of the investigations of structural and phase transformations, a number of important conclusions follows. First, in the region between room temperature and 573 K, a deviation from the linear behavior is observed beginning from ~500 K up to 570 K, after which a sharp drop takes place (Figs. 2, 3). As was already noted, these temperatures can be considered as the threshold temperatures of the onset (T_{sr}) and, correspondingly, the completion (in the given thermal regime) of the process of nanocrystallization of the amorphized alloy, which occurs via the growth of numerous centers, i.e., nanocrystals that already exist in them in the initial state after HPT. These temperatures proved to be close for all the samples that were studied and qualitatively agree with the DSC data (see Fig. 8).

Second, the linear $\rho(T)$ dependence of the $Ti_{49.5}Ni_{50.5}$ alloys upon cooling from 573 K is broken by the existence of two inflections at M_s' and M_f' due to the $B2 \rightarrow R$ transition (see insets in Figs. 2 and 3). The subsequent heating to temperatures that exceed 620–630 K demonstrates a sharp decrease in $\rho(T)$ and, on the contrary, a jump in the heat release in the DSC curves in the temperature range to 680 K, which in this case, according to the TEM data, are caused by the process of primary recrystallization. Then, in the plateau of the DSC curve, the jump is caused by the process of normal grain growth (via competitive growth of nanograins), which is subsequently replaced by the anomalous growth of some SMC grains (process of secondary recrystallization). Upon the subsequent isochronous annealing, this mechanism is exhausted, and the stage of normal grain growth gradually returns, which causes the grain sizes to level off at micron dimensions, and hardly affects the $\rho(T)$ dependence. Here, an important role is played by the processes of changing solubility of Ni and by the precipitation and subsequent dissolution of second phases in the alloy at these temperatures [2–7, 23].

With increasing temperature (to 823–873 K) and annealing time, intense growth of the grain size (to average values of 500–600 nm) occurs and many grains reach sizes of 1 μm or even greater (Figs. 7, 9). The phenomenon of this anomalously sharp increase in grain size with increasing annealing temperature from 773 to 873 K (i.e., by only 50–100 K) is by no means usual and required additional more careful investigations. It is known that the $Ti_{49.5}Ni_{50.5}$ alloy in its chemical composition refers to aging alloys [1–7]; in the process of low-temperature annealings and, moreover, upon devitrification, coherent β' particles (of the Guinier–Preston-zone type) and precipitates of the excessive X phase (Ti_3Ni_4) are formed in it, in particular along grain boundaries [16, 23]. They have been revealed by electron microscopy and from the identification of a whole number of SAED patterns.

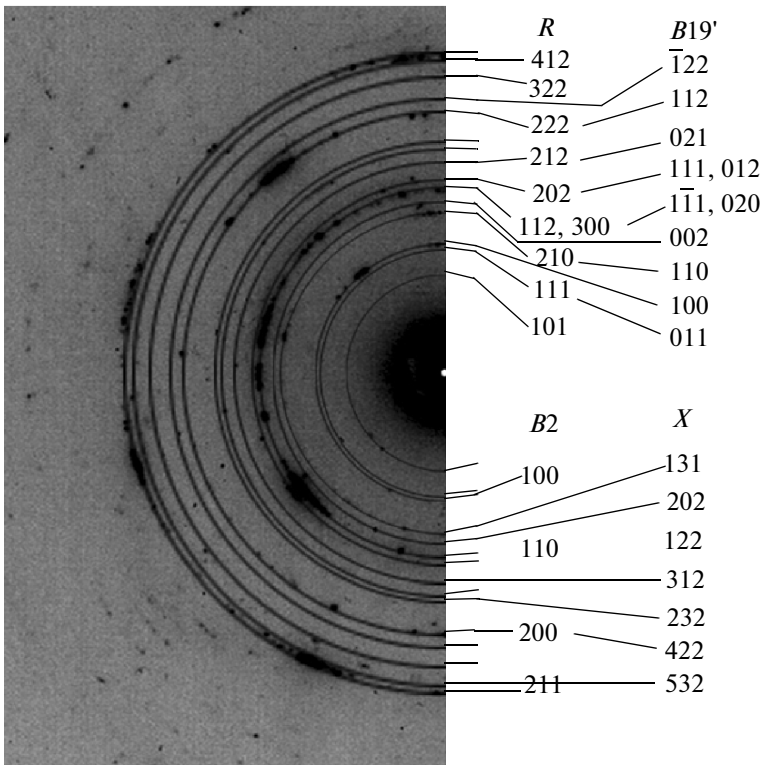

Fig. 10. Typical SAED pattern of the $Ti_{49.5}Ni_{50.5}$ alloy subjected to HPT and to annealing at 773 K. Diffraction reflections of the *B*2, *R*, and *B*19' phases and of the aging *X* phase (Ti_3N_4) are presented.

One of these patterns, along with the scheme of identification, is given in Fig. 10. It should be emphasized that, in this scheme, the *hkl* indices of reflections of almost all possible phases are indicated as follows: austenite, *B*2 TiNi; aging *X* phase (Ti_3Ni_4); martensitic phases *R* and *B*19'. It can be seen that many of these reflections nearly coincide. With allowance for the data obtained by the methods of X-ray diffraction, temperature measurements of electrical resistivity, differential scanning calorimetry, scanning electron microscopy, and transmission electron microscopy in situ, a conclusion was drawn regarding the presence of the following phases in the alloy subjected to low-temperature annealings: basic matrix phase *B*2 TiNi; and second phases TiC(N), $Ti_4Ti_2O_x$, and *X*-Ti_3Ni_4 (in amounts of no more than 1 wt % each). The possible presence of a certain amount of the martensitic phase *R* TiNi and *B*19' TiNi at room temperature was also taken into account, which may be related to the conditions of sample preparation for electron microscopy.

It is evident that the preferential presence of highly disperse *X* particles enriched in nickel at the boundaries and subboundaries of grains will suppress grain growth upon low-temperature annealings. If, at a higher annealing temperature (more than 823 K) these particles begin coalescing and then partly dissolving, they will stop causing the blocking (barrier) action on the grain growth, which will lead to an accelerated growth of their dimensions.

Third, the last cycle of cooling (773 K to T_N) and heating (T_N – 323 K) in all cases is characterized by specific bends in the $\rho(T)$ curves, which are caused by the forward and reverse TMTs ($B2 \leftrightarrow R \leftrightarrow B19'$, Figs. 2, 3). The characteristic temperatures of the TMTs in the alloys studied have been determined by the two-tangent method and are given for some samples in Tables 1 and 2. Figure 11 displays analogous $\rho(T)$ and $\chi(T)$ curves for the $Ti_{49.5}Ni_{50.5}$ alloy subjected to HPT ($n = 5$) and subsequent isothermal annealings for 1 h at various temperatures (at 573 K, curve *1* corresponds to the center of the disk and curve *2* corresponds to its edge; at 623 K, curve *3* corresponds to the center of the disk and curve *4* corresponds to the edge; and, at 723 K, curve *5* corresponds to the edge of the disk). The thermal cycles were performed according in the following series: $RT \rightarrow T_N$ (T_{He} for $\chi(T)$) $\rightarrow$ 400 K $\rightarrow$ $T_N(T_{He}) \rightarrow RT$.

Thus, severe plastic deformation using HPT at room temperature produces in metastable TiNi-based alloys that exist in both austenitic (*B*2) and martensitic states an almost complete amorphization after five (and more so, after ten) revolutions of the anvil [26]. The isolated nanocrystalline inclusions with dimensions of 10–50 nm that are retained in large amounts in the amorphous matrix can undergo a $B2 \rightarrow R$ TMT

Table 1. Temperatures of the start and finish of the forward and reverse martensitic transformations $B2 \leftrightarrow R$ and $R \leftrightarrow B19'$ in the $Ti_{49.5}Ni_{50.5}$ alloy after deformation by HPT and subsequent heating

Treatment	Martensitic points, K							
	Transitions $B2 \leftrightarrow R$				Transitions $R \leftrightarrow B19'$			
	M'_s	M'_f	A'_s	A'_f	M_s	M_f	A_s	A_f
1. HPT at RT, $n = 5$ rev								
Disk center	–	–	–	–	–	–	–	–
Heating to 573 K for 20 min	310	290	305	315	–	–	–	
Heating to 773 K for 20 min	309	295	295	310	235	195	285	300
Disk edge	–	–	–	–	–	–	–	–
Heating to 573 K for 20 min	310	290	305	315	–	–	–	–
Heating to 773 K for 20 min	305	295	305	310	230	185	280	295
2. HPT at RT, $n = 10$ rev								
Disk center	–	–	–	–	–	–	–	–
Heating to 573 K for 20 min	315	290	295	320	–	–	–	–
Heating to 773 K for 20 min	305	290	295	310	230	185	265	290

Table 2. Critical temperatures of the martensitic transitions $B2 \leftrightarrow R \leftrightarrow B19'$ depending on the average grain size in the $Ti_{49.5}Ni_{50.5}$ alloy

Annealing temperature, K	d_{av}, μm	M'_s, K	M'_f, K	A'_s, K	A'_f, K	M_s, K	M_f, K	ΔM	A_s, K	A_f, K	ΔA	$\Delta(A\text{-}M)$
573	0.03	315	290	305	320	–	–	–	–	–	–	–
673	0.05	315	295	300	320	180	130	50	210	250	40	120
773	0.07	310	295	300	315	200	140	60	240	270	30	130
823	0.10	305	295	300	310	220	160	70	260	290	30	130
873	0.18	305	295	300	310	270	220	50	290	315	25	95
before HPT	35	–	–	–	–	280	250	30	290	310	20	60

upon cooling or deformation, which in its structural characteristics is close to a second-order phase transition. However, the $B2(R) \rightarrow B19'$ TMT is in fact absent in these inclusions upon cooling down to very low temperatures.

The total $B2 \rightarrow R \rightarrow B19'$ TMTs, which are responsible for the significant SME, appear in these HPT alloys if they had been preliminarily subjected to annealing. Based on the results of electron-microscopic investigations, we can speak of the presence of a first critical size, below which no martensitic transformations occur in the alloy. In nanograins 20–50 nm in size, both in isolated grains in the amorphous matrix and in the nanostructured alloys, only the $B2 \leftrightarrow R$ TMTs are possible. In grains of greater size (≥50 nm), cascade TMTs $B2 \leftrightarrow R \leftrightarrow B19'$ are possible. The following, or second critical size, on the order of 50 nm (for R martensite) or 100 nm (for $B19'$ martensite) is related to the mechanism of self-accommodation of volume changes and anisotropic stresses in nan-

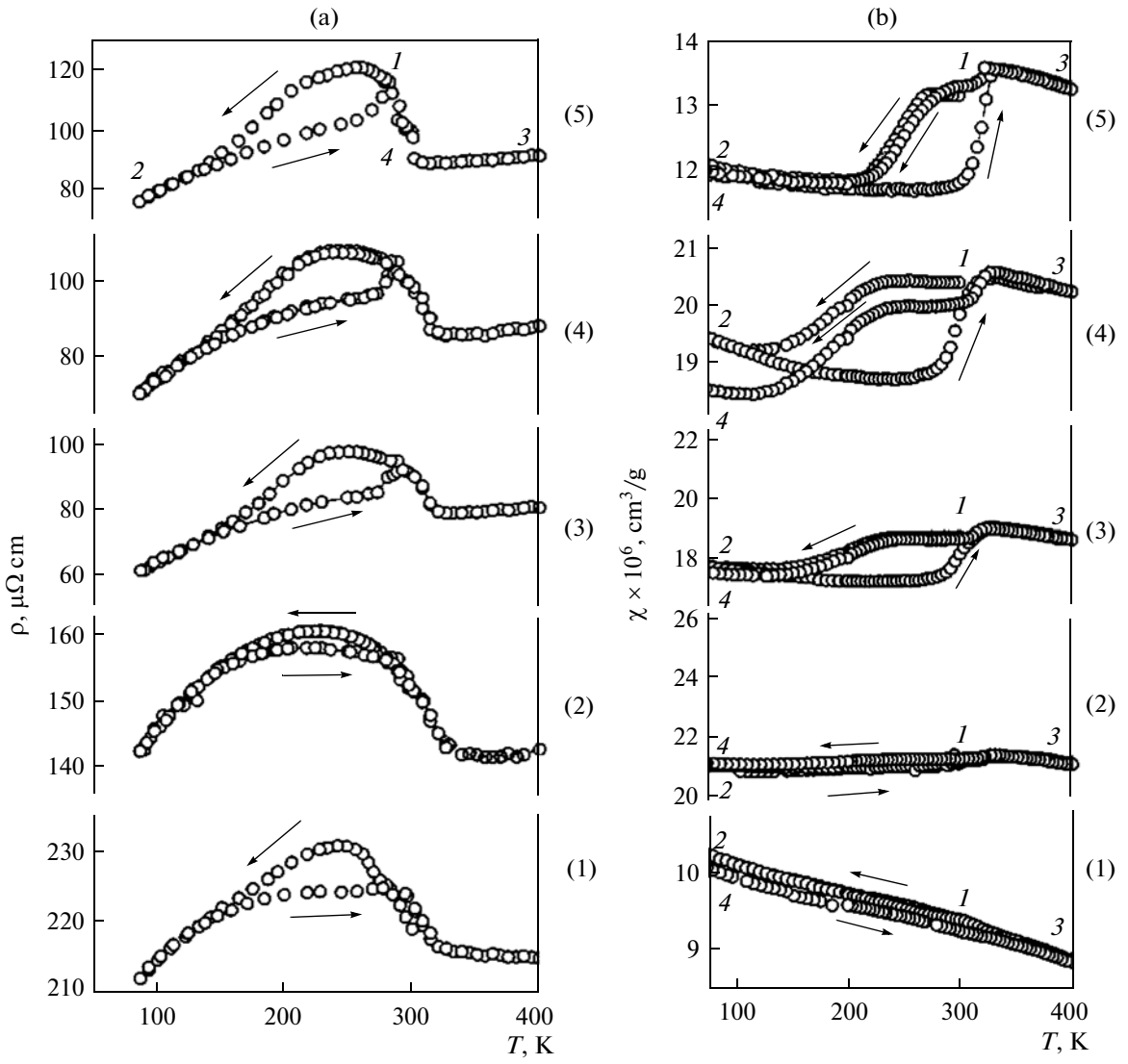

Fig. 11. Temperature dependences of (a) electrical resistivity $\rho(T)$ and (b) magnetic susceptibility $\chi(T)$ of $Ti_{49.5}Ni_{50.5}$ alloy subjected to HPT at room temperature (with $n = 5$ rev and $P = 6$ GPa) and to subsequent isothermal annealing for 1 h at 573 K (1. center of the disk; 2. edge of the disk), 623 K (3. center; 4. edge), and 723 K (5. edge of the disk).

ograins, which are due to the martensitic transformation, namely, to the possible additive twinning of martensite crystals inside the nanograins. In nanograins whose dimensions exceed them, the $B2 \leftrightarrow R$ and $B2 \leftrightarrow R \leftrightarrow B19'$ transformations under certain conditions are accompanied by the formation of single-packet twinned martensite morphology. The morphology only becomes multipacket in grains of substantially greater size (on the order of a micron or greater, according to our estimates), which is analogous to that observed in conventional polycrystalline alloys.

It follows from a comparison of the results obtained that, first, the metastable nanostructured alloy $Ti_{49.5}Ni_{50.5}$ undergoes a two-stage TMT $B2 \leftrightarrow R \leftrightarrow B19'$. Second, in this case the position of the characteristic temperatures of the first transition $B2 \leftrightarrow R$ in them always is increased somewhat (see Fig. 12, Tables 1, 2). However, in the second transition $B2(R) \leftrightarrow B19'$, a stabilization effect is clearly observed that consists of a decrease in all the temperatures, which is somewhat greater for the forward transformation and somewhat smaller for the reverse transformation (Fig. 12; Tables 1, 2). Third, the controlled annealing of the alloys after HPT, with the retention of the nanostructured state, makes it possible to precisionally control the temperatures of the martensitic transitions. The effect of a maximum stabilization at close dimensions of nanograins is achieved in the alloys supersaturated with nickel, including the alloy under study.

The room-temperature tensile tests of the $Ti_{49.5}Ni_{50.5}$ alloy subjected to HPT have shown that, compared to the conventional alloys of the same compositions, the nanostructured alloys have substantially

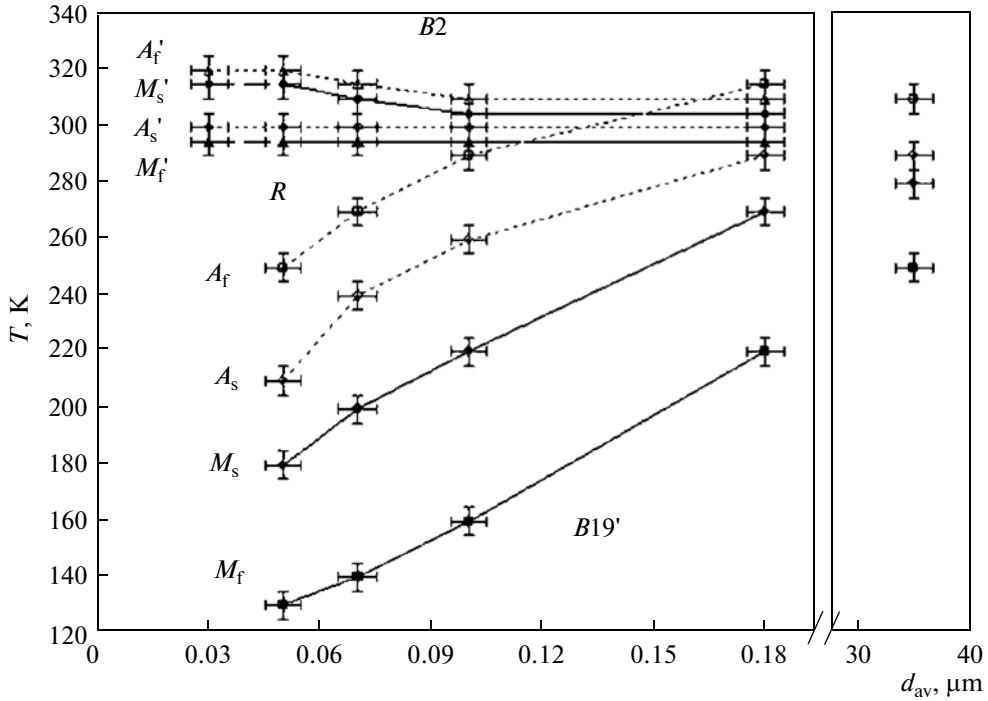

Fig. 12. Dependences of critical temperatures of $B2 \leftrightarrow R$ and $B2 \leftrightarrow B19'$ martensitic transformations upon cooling (heating) on average grain size in nanostructured $Ti_{49.5}Ni_{50.5}$ alloy.

higher strength properties, though smaller plasticity (Fig. 13, curves *1*, *2*, respectively). The nanocrystallization leads to record high values of the ultimate strength (to 2700 MPa), yield strength (1700 MPa), and reactive stress (1300–1500 MPa) at a satisfactory relative elongation (to 20%) (Fig. 13, curve *3*). Moreover, the alloy subjected to HPT demonstrates a very attractive structural stability and attractive mechanical properties in the austenitic state at enhanced temperatures of tensile tests (673–723 K), at which the nanostructured materials can manifest superplastic behavior. The tensile tests at strain rates of 10^{-3} and 10^{-4} s^{-1} at 673 K show that the TiNi alloy subjected to HPT retains strength properties (to 1800 and 1500 MPa, respectively) that are higher than those observed in the initial (undeformed after HPT) state (Fig. 13, curve *1*; Fig. 14). In this case, fairly high relative elongation at fracture (to 30 and 100%, respectively) was also achieved. As the deformation temperature increases to 773 and 923 K, the strength properties (yield stress and ultimate strength) decrease naturally, especially at 923 K. In particular, this decrease can be due to growth in the grain size in the process of testing at enhanced temperatures. At a strain rate of 10^{-3} s^{-1}, a maximum elongation more than 200% was reached at 773 K, as well as at a large strain hardening and an ultimate strength more than 900 MPa (Fig. 14).

To conclude, we note special, yet undoubtedly universal, mechanisms of self-accommodation (adaptation) of elastic stresses and distortions of the crystal lattice upon martensitic transformations, e.g., the ability of martensite to inherit defects that exist in the initial austenite without a strong change in the critical parameters and shear mechanisms of martensitic transformations, despite their variety in TiNi-based alloys. These specific mechanisms appear to have three main causes, i.e.,

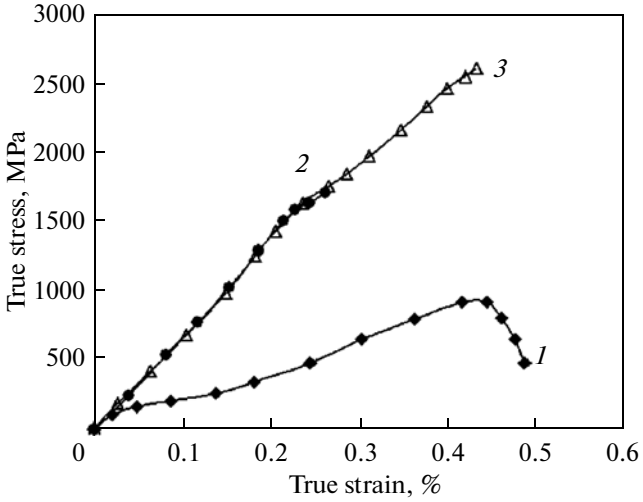

Fig. 13. Effect of various treatments on the mechanical properties of the $Ti_{49.5}Ni_{50.5}$ alloy at room temperature (strain rate is 10^{-3} s^{-1}): (◆) as-quenched; (●) after HPT; and (△) after HPT + annealing at 473 K for 0.5 h.

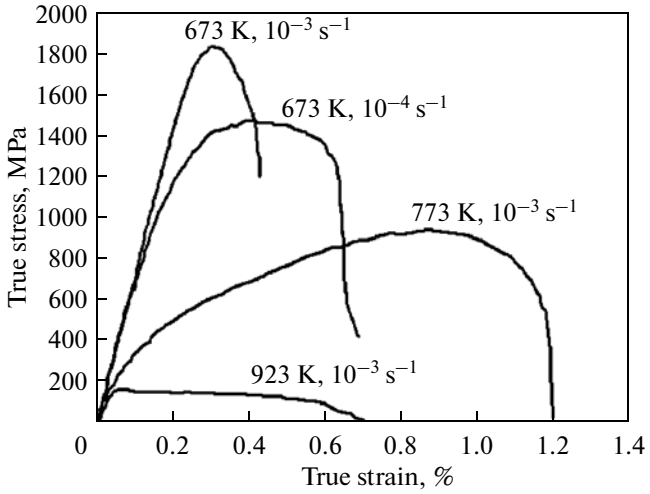

Fig. 14. True stress–true strain curves of $Ti_{49.5}Ni_{50.5}$ alloy after HPT at enhanced temperatures.

(1) the strong and quasi-isotropic softening of all elastic moduli of the *B*2 austenite and of martensitic phases in the metastable state;

(2) the first-order phase transitions in them begin to develop as second-order transitions and, primarily, the minimum specific negative volume changes and sign-anisotropic linear changes under the conditions of high interphase and intercrystallite coherence of the lattices of austenite and martensite in the temperature-, deformation-, and force-related ranges of transformations;

(3) the thermoelastic nature and the corresponding mechanisms of these transitions, in which the elastic energy stored during the forward transition becomes a significant driving force for the reverse transition, thereby substantially narrowing its hysteresis.

It has been revealed that this general principle works not only under the conditions of a multipacket hierarchy of coherent twinned crystals, but also in the nanocrystalline state. In this case, even if the neighboring austenite grains are oriented arbitrarily, which is partly inherited by the arising martensite, the elastic energy is minimized, but continues to be stored. In conventional polycrystalline alloys, as is well-known, the thermoelasticity can easily be spoiled by forcibly disturbing the self-accommodated hierarchy of separate martensitic crystals oriented relative to one another in a twinning manner, e.g., by eliminating their elastic-plastic adaptation through plastic deformation. However, in high-strength nanostructured alloys, this effect of thermoelasticity becomes spontaneous and difficult to eliminate because of the high values of the limits of phase and deformation-related yield, thereby demonstrating another important advantage of nanostructured alloys with SME.

CONCLUSIONS

The main most important results of complex systematic investigations performed in this work are as follows.

(1) It has been shown that the technology of producing nanocrystalline materials using the low-temperature annealing of TiNi-based alloys amorphized by HPT occupies a special place, which makes it possible to precisionally control the average size of nanograins in very narrow limits (10–100 nm). These nanocrystalline TiNi-based alloys demonstrate high strength; undergo a mechanically induced thermoelastic martensitic transformation; possess a shape-memory effect with large reactive forces necessary to create high-force elements of shape-memory constructions; and exhibit high thermomechanical reliability, durability, wear resistance, and corrosion resistance.

(2) It has been revealed that a unique and practically important feature of thermoelastic martensitic transformations in TiNi-based alloys is their relatively weak sensitivity to the dimensions of nanograins and to various nano- and submicrocrystalline states upon the manifestation of the size effect on the stabilization of austenite. Upon cooling, in the TiNi alloy, the $B2 \leftrightarrow R$ transition occurs in nanograins with dimensions of ~20 nm and greater, even in the presence of the surrounding amorphous matrix; in nanograins, with sizes twofold larger (~50 nm), $B2 \leftrightarrow R \leftrightarrow B19'$ martensitic transitions become possible upon cooling, which are responsible for large and practically important shape-memory effects in these alloys. When the martensitic transformations are induced by force action, these critical sizes become even smaller by a factor of two.

(3) The direct in situ observations of martensitic transformations in such small grain–crystallites in titanium nickelide alloys, just as before in rapidly quenched TiNi-based alloys [11], reveal another important and unique feature, i.e., the nucleation and growth of martensitic crystals through the austenite single-nano-crystal–martensite single-nano-crystal mechanism without internal twinning with an invariant lattice. It has been shown that this mechanism of martensitic phase rearrangement of the atomic crystal lattice via pure shear takes place mainly in nanograins with dimensions of 50–100 nm, while in coarser submicrocrystalline grains an additional mechanism is switched on, i.e., the twinning self-accommodation of bulk linearly anisotropic stresses caused by the martensitic transition, which occurs via deformationally adaptive single-packet elastic nanotwinning through standard shear systems that act in these alloys, but primarily through the mechanical-twinning system $(001)_m \,||\, \{110\}_{B2}$.

(4) Nanocrystallization leads to record high values of the ultimate strength (to 2700 MPa); yield stress (1700 MPa); and, correspondingly, reactive stress

upon the realization of the shape–memory effect (1300–1500 MPa) with a significant relative elongation (to 20%) at room temperature, as well as at enhanced temperature of tensile tests (to 673–723 K), and with the manifestation of superplastic behavior (elongation at fracture on the order of 200%) at 773 K.

ACKNOWLEDGMENTS

This work was supported in part by the Presidium of the Russian Academy of Sciences (project no. 12-P-2-1060), by the Presidium of the Ural Branch of the Russian Academy of Science (projects nos. 12-2-005-Arktika, 12-2-007-DMU) and by the Russian Foundation for Basic Research (project no. 11-02-00021).

REFERENCES

1. K. Otsuka, K. Shimizu, Y. Suzuki, Y. Sekiguchi, C. Tadaki, T. Honma, and S. Miyazaki., *Shape Memory Alloys*, E. by H. Funakubo (Kyoto, 1984; Metallurgiya, Moscow, 1990).
2. V. N. Khachin, V. G. Pushin, and V. V. Kondrat'ev, *Titanium Nickelide: Structure and Properties* (Nauka, Moscow, 1992) [in Russian].
3. V. G. Pushin, V. V. Kondrat'ev, and V. N. Khachin, *Pretransition Phenomena and Martensite Transformations* (Ural. Otd. Ross. Akad. Nauk, Ekaterinburg, 1998) [in Russian].
4. *Shape Memory Materials,* Ed. by K. Otsuka and C. M. Wayman (Cambridge University Press, Cambridge, 1999).
5. V. N. Zhuravlev and V. G. Pushin, *Alloys with Thermomechanical Memory and Their Application in Medicine* (Ural. Otd. Ross. Akad. Nauk, Ekaterinburg, 2000) [in Russian].
6. V. G. Pushin, S. D. Prokoshkin, R. Z. Valiev, V. Brailovskii, E. Z. Valiev, A. E. Volkov, A. M. Glezer, S. V. Dobatrin, E. F. Dudarev, V. T. Zhu, Yu. G. Zainulin, Yu. R. Kolobov, V.V. Kondratiev, A. V. Korolev, A. I. Korshunov, N. I. Kourov, N. V. Kudrevatykh, A. I. Lotkov, L. L. Meisner, A. A. Popov, N. N. Popov, A. I. Razov, M. A. Khusainov, Yu. I. Chumlyakov, S. V. Andreev, A. A. Baturin, S. P. Belyaev, V. N. Grishkov, D. V. Gunderov, A. P. Dyupin, K. V. Ivanov, V. I. Itin, M. K. Kasymov, O. A. Kashin, I. V. Kireeva, A. I. Kozlov, T. E. Kuntsevich, N. N. Kuranova, N. Yu. Pushina, E. P. Ryklina, A. N. Uksusnikov, I. Yu. Khmelevskaya, A. V. Shelyakov, V. Ya. Shklover, E. V. Shorokhov, and L. I. Yurchenko, *Titanium Nickelide Alloys with Shape Memory. Ch. I. Structure, Phase Transformations and Properties* (Ural. Otd. Ross. Akad. Nauk, Ekaterinburg, 2006) [in Russian].
7. V. G. Pushin, "Alloys with a thermomechanical memory: Structure, properties and application," Phys. Met. Metallogr. **90** (Suppl. 1), S68–S95 (2000).
8. S. D. Prokoshkin, V. G. Pushin, E. P. Ryklina, and I. Yu. Khmelevskaya, "Application of titanium nickelide-based alloys in medicine," Phys. Met. Metallogr. **97** (Suppl. 1), S56–S96 (2004).
9. V. Brailovski, I. Yu. Khmelevskaya, S. D. Prokoshkin, V. G. Pushin, E. P. Ryklina, and R. Z. Valiev, "Foundations of heat and thermomechanical treatments and their effect on the structure and properties of titanium nickelide-based alloys," Phys. Met. Metallogr. **97** (Suppl. 1), S3–S55 (2004).
10. V. G. Pushin, "Structures, properties, and application of nanostructured shape memory TiNi-based alloys," in *Nanomaterials by Severe Plastic Deformation*, Ed. by M. Zehetbauer and R. Valiev (Wiley, Weinheim, 2004), pp. 822–828.
11. V. G. Pushin, S. B. Volkova, and N. M. Matveeva, "Structural and phase transformations in quasi-binary TiNi–TiCu alloys rapidly quenched from the melt: I. High-copper amorphous alloys," Phys. Met. Metallogr. **83**, 275–282 (1997); V. G. Pushin, S. B. Volkova, and N. M. Matveeva, "Structural and phase transformations in quasi-binary TiNi–TiCu alloys rapidly quenched from the melt: II. Alloys with mixed amorphous–crystalline structure," Phys. Met. Metallogr. **83**, 283–288 (1997); V. G. Pushin, S. B. Volkova, and N. M. Matveeva, "Structural and phase transformations in quasi-binary TiNi–TiCu alloys rapidly quenched from the melt: III. Mechanisms of crystallization," Phys. Met. Metallogr. **83**, 435–443 (1997); V. G. Pushin, S. B. Volkova, and N. M. Matveeva, "Structural and phase transformations in quasi-binary TiNi–TiCu alloys rapidly quenched from the melt: IV. The microstructure of crystalline alloys," Phys. Met. Metallogr. **83**, 673–678 (1997); V. G. Pushin, S. B. Volkova, N. M. Matveeva, L. I. Yurchenko, and A. S. Chistyakov, "Structural and phase transformations in quasi-binary TiNi–TiCu alloys rapidly quenched from the melt: V. Effect of heat treatment," Phys. Met. Metallogr. **83**, 679–683 (1997).
12. V. G. Pushin, V. V. Stolyarov, R. Z. Valiev, N. I. Kourov, N. N. Kuranova, E. A. Prokofiev, and L. I. Yurchenko, "Features of structure and phase transformations in shape memory TiNi-based alloys after severe plastic deformation," Annales de Chimie Sci. Mater. **27** (3), 77–88 (2002).
13. V. G. Pushin, V. V. Stolyarov, R. Z. Valiev, N. I. Kourov, N. N. Kuranova, E. A. Prokofiev, and L. I. Yurchenko, "Development of methods of severe plastic deformation for the production of high-strength alloys based on titanium nickelide with a shape-memory effect," Phys. Met. Metallogr. **94** (Suppl. 1), S54–S68 (2002).
14. V. G. Pushin, R. Z. Valiev, and L. I. Yurchenko, "Processing of nanostructured TiNi-shape memory alloys: Methods, structures, properties, application," J. Phys. IV France **112**, 659–662 (2003).
15. V. G. Pushin and R. Z. Valiev, "The nanostructured TiNi shape memory alloys: New properties and applications," Solid State Phenom. **94**, 12–21 (2003).
16. R. Z. Valiev, V. G. Pushin, D. V. Gunderov, and A. G. Popov, "The use of severe deformations for preparing bulk nanocrystalline materials from amorphous alloys," Phys.-Dokl. **49**, 519–521 (2004).
17. S. D. Prokoshkin, I. Yu. Khmelevskaya, S. V. Dobatkin, I. B. Trubitsyna, E. V. Tatyanin, V. V. Stolyarov, and E. A. Prokofiev, "Alloy composition, deformation temperature, pressure and post-deformation annealing effects in severely deformed Ti–Ni based shape memory alloys," Acta Mater. **53**, 2703–2714 (2005).

18. R. Z. Valiev, D. V. Gunderov, and V. G. Pushin, "Metastable nanostructured SPD TiNi alloys with unique properties," J. Metastable Nanostruct. Mater. **24–25**, 7–12 (2005).
19. V. G. Pushin, R. Z. Valiev, Y. T. Zhu, D. V. Gunderov, N. I. Kourov, T. E. Kuntsevich, A. N. Uksusnikov, and L. I. Yurchenko, "Effect of severe plastic deformation on the behavior of Ti–Ni shape memory alloys," Mater. Trans. **47**, 694–697 (2006).
20. E. Prokofiev, D. Gunderov, A. Lukyanov, V. Pushin, and R. Valiev, "Mechanical behavior and stress-induced martensitic transformation in nanocrystalline $Ti_{49.4}Ni_{50.6}$ alloy," Mater. Sci. Forum **584–586**, 470–474 (2008).
21. R. Valiev, D. Gunderov, E. Prokofiev, V. Pushin, and Yu. Zhu, "Nanostructuring of TiNi alloy by SPD processing for advanced properties," Mater. Trans. **49**, 97–101 (2008).
22. D. V. Gunderov, N. N. Kuranova, A. V. Luk'yanov, A. N. Uksusnikov, E. A. Prokof'ev, L. I. Yurchenko, R. Z. Valiev, and V. G. Pushin, "Application of severe plastic deformation by torsion to form amorphous and nanocrystalline states in large-size TiNi alloy sample," Phys. Met. Metallogr. **108**, 131–138 (2009).
23. N. N. Kuranova, D. V. Gunderov, A. N. Uksusnikov, A. V. Luk'yanov, L. I. Yurchenko, E. A. Prokof'ev, V. G. Pushin, and R. Z. Valiev, "Effect of heat treatment on the structural and phase transformations and mechanical properties of TiNi alloy subjected to severe plastic deformation by torsion," Phys. Met. Metallogr. **108**, 556–568 (2009).
24. N. N. Kuranova, V. V. Makarov, V. G. Pushin, A. N. Uksusnikov, R. Z. Valiev, D. V. Gunderov, A. V. Luk'yanov, and E. A. Prokof'ev, "Amorphization of bulk TiNi-based alloys by severe plastic deformation under high pressure torsion," Bull. Russ. Acad. Sci.: Phys. **73**, 1117–1119 (2009).
25. V. G. Pushin, N. N. Kuranova, N. I. Kourov, R. Z. Valiev, E. Z. Valiev, V. V. Makarov, A. V. Pushin, and A. N. Uksusnikov, "Baroelastic shape memory effects in titanium nickelide alloys subjected to plastic deformation under high pressure," Tech. Phys. **57**, 1106–1114 (2012).
26. V. G. Pushin, R. Z. Valiev, E. Z. Valiev, N. I. Kourov, N. N. Kuranova, V. V. Makarov, A. V. Pushin, and A. N. Uksusnikov, "Phase and structural transformations in the $Ti_{49.5}Ni_{50.5}$ alloy with a shape-memory effect during torsion under high pressure," Phys. Met. Metallogr. **113**, 256–270 (2012).

Translated by S. Gorin